Available online at www.sciencedirect.com
SCIENCE DIRECT®
ELSEVIER
Journal of Magnetism and Magnetic Materials 260 (2003) 282–294
Journal of magnetism and magnetic materials
www.elsevier.com/locate/jmmm

The effects of Ag underlayer and Pt intermediate layers on the microstructure and magnetic properties of epitaxial FePt thin films

Yu-Nu Hsu[a,*], Sangki Jeong[a], David E. Laughlin[a], David N. Lambeth[b]

[a] *Department of Material Science and Engineering, Data Storage Systems Center, Carnegie Mellon University, Pittsburgh, PA 15213-3890, USA*

[b] *Department of Electrical and Computer Engineering, Carnegie Mellon University, Pittsburgh, PA 15213-3890, USA*

Received 18 December 2001; received in revised form 2 July 2002

Abstract

In this work, Ag underlayers, which have a slightly larger lattice parameter than FePt, were found not only to induce epitaxial growth of the FePt films but also to reduce the temperature at which the atomic ordering occurred. Without using the Ag underlayer, the FePt film deposited onto the hydrofluoric acid etched-Si substrate was FCC disordered. When Ag underlayers were used the FePt unit cells were expanded in the film plane. This caused the shrinkage of the FePt unit cells along the film normal direction and resulted in the in situ ordering of the FePt thin film at reduced temperatures. Furthermore, it was found that the degree to which the FePt unit cells contracted along the film normal varied when a Pt intermediate layer was added. This resulted in FePt thin films with different textures and magnetic properties. The microstructural and magnetic properties of the FePt films prepared at various substrate temperatures, FePt thicknesses, Ag underlayer thicknesses and with the use of the Pt intermediate layer were studied to investigate the $L1_0$ FePt ordering.

PACS: 75.70.−i; 75.75.+a

Keywords: FePt magnetic layer; Ag thin film; Pt thin film; Longitudinal recording media; Perpendicular recording media

1. Introduction

The popularity of the computer internet and mobile digital recording devices has further increased the demand of high recording density to store data. In order to increase storage density, the volume of each bit cell has reduced dramatically and consequently heightened the concerns related to recording medium thermal stability. If recording media are in a state of thermal instability, the media can lose stored data easily. The product of the anisotropy energy (K_u) and the volume of the magnetic switching unit (V) represents the energy barrier to magnetization reversal in the presence of a thermal fluctuations. If $K_uV/kT < \sim 60$, the magnetic medium is considered thermally unstable (T: temperature and k: Boltzmann constant) [1]. At high recording

*Corresponding author. Tel.: +1-412-682-5560; fax: +1-412-682-5540.

E-mail address: hsu@icmechanics.com (Y.-N. Hsu).

0304-8853/03/$ - see front matter © 2002 Published by Elsevier Science B.V.
PII: S0304-8853(02)00587-5

density, the volume of the magnetic switching unit (V) becomes smaller. Hence, it is essential to search for new materials that have higher anisotropy energy (K_u) to continue to increase the magnetic recording density.

$L1_0$ FePt is known to have an anisotropy energy (K_u) 15 times higher than the current HCP Co magnetic recording material [2]. It is this large magnetocrystalline anisotropy that has drawn considerable attention to the $L1_0$ FePt thin films as a potential high-density magnetic recording material [3]. FePt *has* FCC phase above 1300°C [4]. At temperatures below 1300°C, the FePt transforms to the $L1_0$ phase, which has its c-axis slightly smaller than its a- and b-axis as shown in Fig. 1. The easy axis of the $L1_0$ FePt phase is along the c-axis direction. The FePt thin film deposited directly onto an amorphous substrate tends to have the FCC structure. This FCC FePt thin film is (1 1 1) textured because the (1 1 1) plane is its close-packed plane. After the FCC (1 1 1) textured FePt thin film is annealed and becomes $L1_0$ ordered, the easy axis is tilted 35° out of the film plane. This was shown by Ristau et al. where FePt thin films deposited onto glass substrates were FCC disordered and (1 1 1) textured [5]. In that work, the FePt film had to be annealed at a temperature greater than 550°C in order to obtain the $L1_0$ ordered phase [5].

In order to use FePt as recording media, the $L1_0$ FePt ordering temperature needs to be reduced and the easy axis should be either perpendicular or parallel to the film plane for perpendicular or longitudinal recording, respectively. In other words, the FePt thin film has to be (0 0 1) textured to function as perpendicular media or (1 0 0) textured to function as longitudinal media.

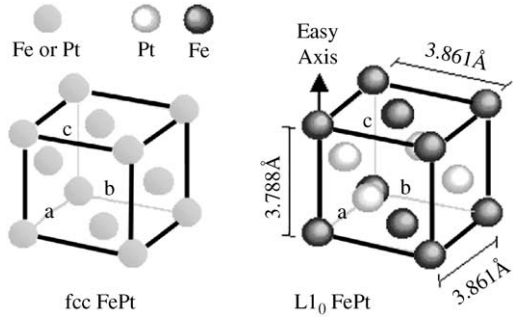

Fig. 1. Schematics of the FePt crystallographic structures of the high temperature FCC phase and the low temperature $L1_0$ phase [6].

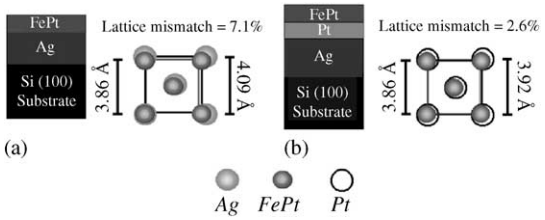

Fig. 2. The schematics of the orientational relationships of (a) FePt (0 0 1) [1 0 0]‖Ag (0 0 1) [1 0 0] and (b) FePt (0 0 1) [1 0 0]‖Pt (0 0 1) [1 0 0].

In this work, underlayers are used to induce the proper texture in FePt thin films and to align the FePt easy axes. We take advantage of the moderate lattice mismatch (7.1%) between Ag and FePt (Fig. 2) and use Ag (0 0 1) underlayers to induce the properly oriented FePt epitaxial films. As reported by Yang et al. [7], single crystal Si (0 0 1) substrates can be used to induce epitaxial growth of Ag (0 0 1) thin films based on the orientational relationship of Ag (0 0 1) [1 1 0]‖Si (0 0 1) [1 1 0]. Furthermore, the lattice misfit of FePt with Pt (2.6%) is even smaller than that with Ag (7.1%). Hence, a Pt intermediate layer has been deposited between the FePt and Ag layers to reduce the film to film lattice misfit. It can be seen that FePt has the cube-on-cube orientational relationship with both Ag and Pt as shown in Fig. 2. In order to further understand the effects of using Ag underlayers and Pt intermediate layers, the microstructural and magnetic properties of the FePt thin films using Ag underlayers as well as Pt intermediate layers were investigated.

Some of the results shown in this paper have been briefly discussed in a previous paper published by the same author [8]. However, this paper is intended to give a very detailed discussion on the effects of the Ag underlayer as well as the Pt intermediate layer.

2. Experiment

There are four variables studied in this work. These four variables are FePt thickness, Ag

thickness, substrate temperature and the use of intermediate layer. To be able to focus on the texture study and exclude the effects of grain size, thin films were all deposited onto single crystal Si (0 0 1) substrates. To remove the oxide layers, the Si (0 0 1) substrates were hydrofluoric acid (HF)-etched [7].

Thin films were deposited by RF diode sputtering in a Leybold-Heraeus Z-400 system. The base pressure was 6×10^{-7} Torr. The atomic composition of the FePt film deposited from a composite target was measured by X-ray fluorescence to be $Fe_{55}Pt_{45}$. The FePt magnetic layers were deposited at a sputtering power density of 0.5 W/cm^2 and Ar pressure of 2.5 mTorr. The Ag and Pt films were deposited with a fixed Argon pressure of 10 mTorr and RF power density of 2.3 W/cm^2. A 12.5 nm Pt intermediate layer was deposited between the FePt magnetic layer and the Ag underlayer. The FePt thickness was varied from 2.5 to 30 nm. The Ag underlayer thickness was varied from 10 to 175 nm. The substrate temperature was changed from 25°C to 300°C.

The magnetic properties of the thin films were measured using a vibrating sample magnetometer (VSM) with fields up to 13 kOe. The orientational relationships between the FePt magnetic layer, Pt intermediate layer and Ag underlayer were investigated by Phillips X'Pert X-ray diffractometer. The textures of these thin films were also studied by Rigaku X-ray $\theta/2\theta$ diffractometer with Cu Kα radiation and a Philips EM 420T transmission electron microscope (TEM).

When the texture was studied by the X-ray diffractometer, only the FePt reflections within the shaded area of Fig. 3 could be accessed [9]. The reflections along the sample normal direction in Fig. 3 can be detected by the X-ray $\theta/2\theta$ diffraction scan. For the $L1_0$ FePt (0 0 1) textured thin film, not only the 002 and 004 fundamental reflections but also the 001 and 003 superlattice reflections can be observed in the X-ray $\theta/2\theta$ diffraction scan (see Fig. 3(a)). On the other hand, for a FePt (1 0 0) textured thin film, only 200 and 400 fundamental reflections can be observed in the X-ray $\theta/2\theta$ diffraction scan (Fig. 3(b)).

If the FePt texture is studied by TEM, the type and relative intensity of the superlattice reflections shown in the TEM diffraction pattern can determine the FePt texture. If the FePt thin film is FCC disordered, only the fundamental reflections can be observed in the TEM diffraction pattern. The superlattice reflections are present when the $L1_0$ ordered phase is formed. The 001 and 110 superlattice reflections are the ones mainly used in this research to determine the $L1_0$ FePt texture. If the $L1_0$ FePt thin film is (1 0 0) or (0 1 0) textured, the 001 superlattice reflections can be observed in the simulated TEM diffraction pattern as shown in Fig. 4(a) and (b). On the other hand, for the $L1_0$ FePt (0 0 1) textured thin film, the 110 superlattice reflections can be observed in the diffraction pattern instead of 001 reflections (see Fig. 4(c)). For the $L1_0$ FePt thin film composed of the $L1_0$ (1 0 0), (0 1 0) and (0 0 1) variants, the TEM diffraction pattern reveals both the 001 and 110 $L1_0$ superlattice reflections as depicted in Fig. 4(d).

As illustrated in Fig. 1, the FePt c-axis becomes slightly shorter than the a- and b-axis during the formation of the $L1_0$ phase. Since FePt $L1_0$

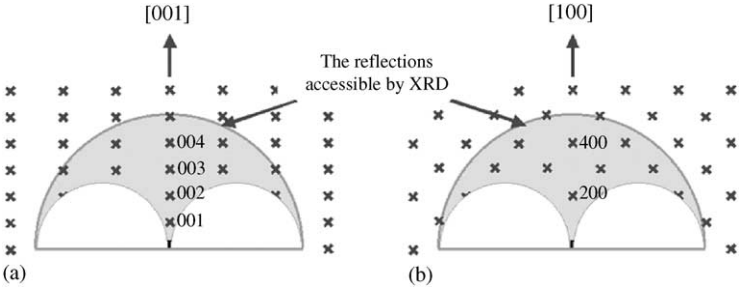

Fig. 3. The FePt reflections accessible by the X-ray $\theta/2\theta$ diffraction scan for the case of the (a) (0 0 1) and (b) (1 0 0) textured thin film [9].

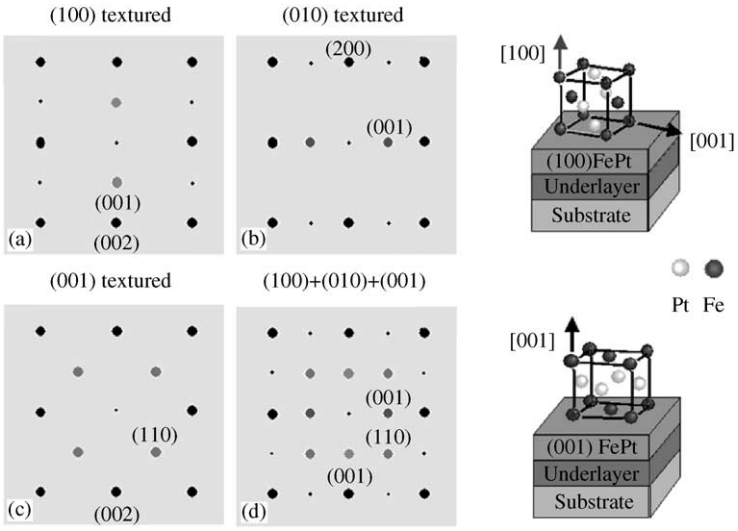

Fig. 4. The simulated TEM diffraction patterns of the $L1_0$ FePt (1 0 0), (1 0 1) and (0 0 1) textured thin films.

ordering is associated with changes of the lattice parameters, it is essential to measure the changes of the FePt lattice parameters. For FePt thin films with strong $L1_0$ ordering, the lattice parameters were obtained from the $L1_0$ (0 0 1), (0 1 0) and (0 0 1) planar spacings. For the FePt thin films with weak $L1_0$ ordering, the $L1_0$ (0 0 1) peak is too weak to be observed by X-ray diffraction. The lattice parameters of those samples were obtained from the $L1_0$ (0 0 2), (0 2 0) and (0 0 2) planar spacings. The FePt lattice parameters of the [0 0 1], [0 1 0] and [1 0 0] axes are twice of the FePt (0 0 2), (0 2 0) and (2 0 0) inter-planar spacings, respectively. The FePt inter-planar spacings were obtained from the peak positions detected by a Phillips X'Pert X-ray diffractometer equipped with a lens that allows X-ray beam to focus when samples are titled along Ψ direction shown in Fig. 5.

The X-ray ϕ-scan is used to detect the in-plane epitaxial relationship between the FePt magnetic layer, Ag underlayer, Pt intermediate layer and Si substarte. The X-ray ϕ-scan is performed by setting the (0 0 2) position in $\theta/2\theta$ and rotating the samples along the ϕ-direction as shown in Fig. 5.

To perform X-ray in-plane diffraction, it is important to make sure that the [1 0 0] axis of the

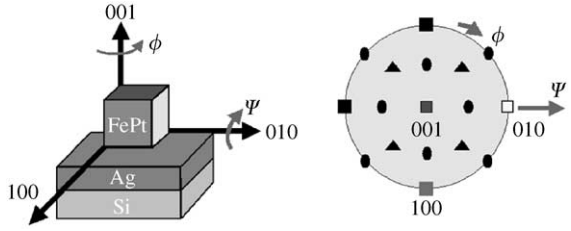

Fig. 5. The measurement setup of obtaining the FePt (2 0 0), (0 2 0) and (0 0 2) inter-planar spacings.

single crystal Si substrate is parallel to the [1 0 0] direction of the sample stage at $\phi = 0$. Hence, X-ray ϕ-scans were first employed to orient in-plane directions of the samples. The FePt (0 0 2) and (0 0 1) inter-planar spacing can then be measured from the X-ray $\theta/2\theta$ diffraction spectrum at zero Φ and Ψ as shown in Fig. 5. The FePt (0 2 0) and (0 1 0) inter-planar spacings can be measured from the X-ray diffraction peak positions by tilting the sample nearly 90° with respect to [0 1 0] axis ($\Psi \sim 90°$) and rotating 90° with respect to [0 0 1] axis ($\Phi = 90°$) as shown in Fig. 5. Likewise, the FePt (2 0 0) and (1 0 0) inter-planar spacing can be measured by the X-ray $\theta/2\theta$ diffraction at the tilting angle of nearly 90° with respect to [0 1 0] axis ($\Psi \sim 90°$) (see Fig. 5).

3. Results and discussion

First, the epitaxial relationships between the FePt magnetic layer, Ag underlayer and the Pt intermediate layer are discussed. Secondly, the results of the effects of FePt thickness, Ag thickness, substrate temperature and the Pt intermediate layer on the FePt microstructure are presented, followed by a discussion of the mechanism of FePt $L1_0$ ordering and texture development. In this section, some hypotheses are proposed to explain the microstructure results at various FePt thickness, Ag thickness, substrate temperature as well as using the Pt intermediate layer. Lastly, the magnetic properties of the FePt thin film are presented.

3.1. Epitaxial relationship investigation

Two samples were studied for the epitaxial relationship investigation. One is the FePt (30 nm)/Ag (175 nm)/Si thin film and the other is the FePt (30 nm)/Pt (12.5 nm)/Ag (175 nm)/Si thin film. The X-ray ϕ-scan spectra of the FePt, Pt, Ag and Si {2 2 0} poles of the thin films along with a (0 0 1) cubic stereographic projection are shown in Fig. 6.

Four Si {4 4 0} diffraction peaks that are 90° apart are observed in the X-ray ϕ-scan spectra shown in Fig. 6(a)–(c). These four peaks correspond to four {1 1 0} poles that are 90° apart in the cubic crystal (0 0 1) stereographic projection. Four Ag, Pt and FePt {2 2 0} diffraction peaks 90° apart are also found in the X-ray ϕ-scan spectra shown in Fig. 6, consistent with the four {1 1 0} poles 90° apart in the cubic crystal (0 0 1) stereographic projection.

For the FePt/Ag/Si and FePt/Pt/Ag/Si thin films, the positions of the four peaks observed in the X-ray ϕ-scans are the same. This indicates that the FePt, Pt, Ag and Si are cube-on-cube oriented as depicted in Fig. 2(a) and (b). As a result, the epitaxial relationship of the FePt/Ag/Si thin film are determined to be FePt [1 1 0] (0 0 1)/Ag [1 1 0] (0 0 1)/Si [1 1 0] (0 0 1). The epitaxial relationship of the FePt/Pt/Ag/Si thin film can also be determined as FePt [1 1 0] (0 0 1)/Pt [1 1 0] (0 0 1)/Ag [1 1 0] (0 0 1)/Si [1 1 0] (0 0 1).

3.2. Microstructural observations

First, the microstructural observations of the FePt thin film directly deposited onto the single crystal Si substrate are presented and compared to

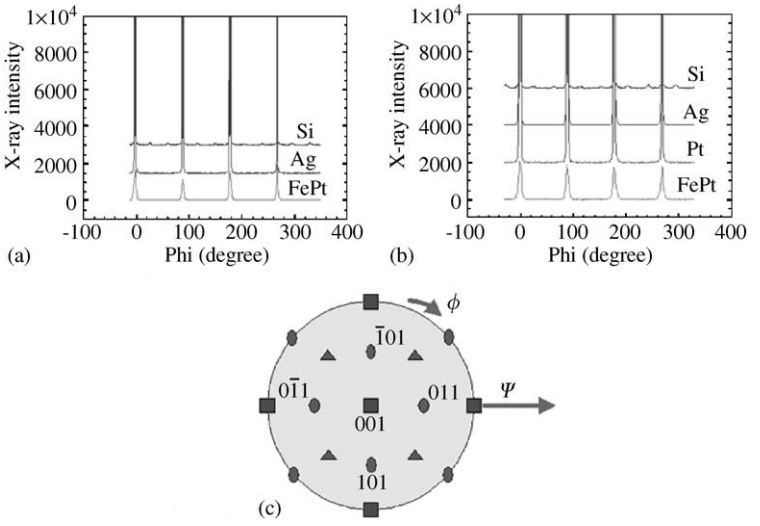

Fig. 6. The X-ray ϕ-scan spectra of the (a) FePt (30 nm)/Ag (175 nm)/Si, (b) FePt (30 nm)/Pt (12.5 nm)/Ag (175 nm)/Si and (c) the stereographic projection of the (0 0 1) textured cubic crystal.

the film deposited onto Ag underlayers. In the second part of this section, the effects of using the Ag underlayer on the FePt $L1_0$ ordering and crystallographic texture are discussed. FePt thickness, Ag thickness and substrate temperature are the three parameters studied here. In the last section, the results of changing the FePt $L1_0$ ordering and texture by using Pt intermediate layers are shown.

For the case when no Ag underlayer is used, a weak FePt (1 1 1) peak is observed by a $\theta/2\theta$ X-ray spectra shown in Fig. 7(a), indicating the FePt film is weakly (1 1 1) textured. From the TEM diffraction pattern of Fig. 7(b), the FePt thin film directly deposited onto the HF-etched Si (0 0 1) single crystal substrate at 300°C is non-epitaxial and displays randomly oriented grains. Therefore, the FePt thin film directly deposited onto the Si substrate is nearly randomly oriented with a weak (1 1 1) texture. In addition, no superlattice reflections of the $L1_0$ ordered phase are observed in the TEM diffraction pattern in Fig. 7(b). Hence, the as-deposited FePt thin film is FCC disordered in the absence of an Ag underlayer.

The TEM diffraction patterns of the 5 and 30 nm FePt films deposited onto Ag underlayers of the same thickness (175 nm) at 300°C are shown in Fig. 8. The $L1_0$ FePt 110 superlattice reflections are observed in the TEM diffraction pattern of the 5 nm FePt thin film. This TEM diffraction pattern matches with the simulated pattern of the FePt (0 0 1) oriented thin film as shown in Fig. 4, which implies that the FePt thin film is (0 0 1) oriented with the *c*-axis (magnetic easy axis) perpendicular to the film plane. The epitaxial relationship between the 5 nm FePt and Ag is therefore FePt

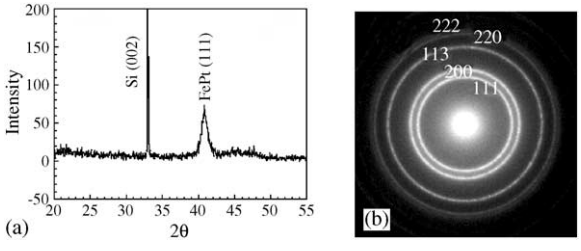

Fig. 7. (a) The $\theta/2\theta$ X-ray diffraction spectrum and (b) the plane-view TEM diffraction pattern of the FePt (30 nm)/Si thin film deposited at 300°C.

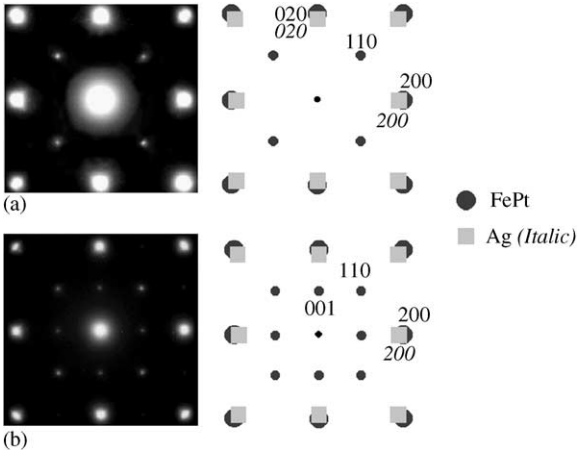

Fig. 8. The TEM diffraction patterns and indexes of the (a) FePt (5 nm)/Ag (175 nm)/Si and (b) FePt (30 nm)/Ag (175 nm)/Si thin films deposited at 300°C.

[1 1 0] (0 0 1)‖Ag [1 1 0] (0 0 1) shown by the TEM diffraction pattern in Fig. 8(a).

The TEM diffraction pattern of the 30 nm FePt thin film shows both the 110 and 001 superlattice reflections (see Fig. 8(b)). This indicates that the 30 nm FePt thin film has its *c*-axis distributed along each of the [1 0 0], [0 1 0] and [0 0 1] directions of the Si single crystal.

The TEM diffraction patterns shows that the 5 nm FePt film has only the $L1_0$ (0 0 1) variant but the 30 nm FePt film has $L1_0$ (0 0 1), (0 1 0) as well as (0 0 1) variants. This suggests that the $L1_0$ FePt (0 0 1) variant is formed before the $L1_0$ FePt (1 0 0) and (0 1 0) variants. In other words, the $L1_0$ FePt (0 0 1) variant is formed at small thicknesses of the FePt layer and the $L1_0$ FePt (1 0 0) and (0 1 0) variants begin to form as the FePt thickness increases.

The TEM selected area diffraction pattern and the simulated pattern of the 30 nm FePt layer deposited onto the 10 nm Ag underlayers are presented in Fig. 9. The $L1_0$ FePt 110 reflections observed in the diffraction pattern of the FePt/Ag (175 nm) film (Fig. 8(b)) are absent in the diffraction pattern of the FePt/Ag (10 nm) thin film. The absence of the $L1_0$ FePt 110 reflections and the appearance of the 001 reflections in the FePt/Ag (10 nm) thin film suggest that this FePt thin film

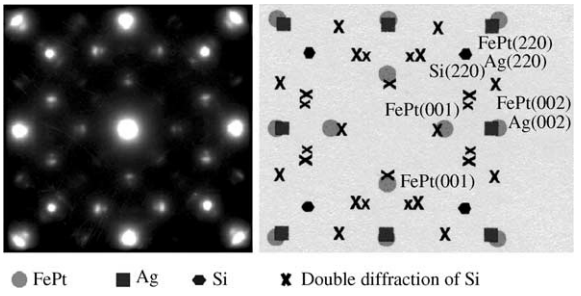

Fig. 9. TEM selected area diffraction patterns and simulated patterns of the FePt (30 nm)/Ag (10 nm) film deposited at 300°C.

has its *c*-axis oriented in the thin film plane. However, the FePt thin film deposited onto the 175 nm thick Ag underlayer has *c*-axis both parallel to and perpendicular to the thin film plane as evidenced by the presence of the 110 and 001 reflections observed in Fig. 8(b).

In addition, the $L1_0$ FePt superlattice reflection intensity of the FePt/Ag (10 nm) thin film is weaker than that of the FePt/Ag (175 nm) thin film. This suggests that the FePt thin film deposited onto the 10 nm thin Ag underlayer is less atomically ordered than that deposited onto the 175 nm thick Ag layer.

Fig. 10 shows the X-ray $\theta/2\theta$ diffraction spectra of the FePt (30 nm)/Ag (175 nm)/HF Si (0 0 1) deposited at various substrate temperatures. At 25°C, Ag (1 1 1) and (0 0 2) peaks are observed in the X-ray $\theta/2\theta$ diffraction pattern. This indicates that the Ag underlayer has a (0 0 2) texture mixed with a weak (1 1 1) texture. This mixed Ag (1 1 1) and (0 0 2) textures result in a mixture of FePt (1 1 1) and (0 0 2) textures as observed by the small FePt (1 1 1) and strong (0 0 2) peaks in Fig. 10. At the substrate temperature of 300°C, the Ag and FePt layers are observed to have only the (0 0 2) peaks in the X-ray $\theta/2\theta$ diffraction spectra. This indicates that the Ag (0 0 2) underlayer induces the epitaxial growth of the FePt (0 0 2) layer. In addition, it can be seen that the $L1_0$ FePt (0 0 1) peak becomes stronger with increasing substrate temperature. This indicates that more $L1_0$ FePt (0 0 1) phase forms at high substrate temperature than at room temperature.

The arcs seen in the electron diffraction pattern of Fig. 11(a) from the FePt/Ag film deposited at

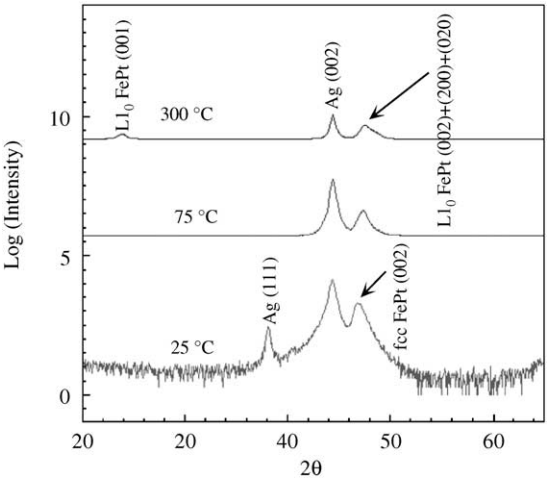

Fig. 10. The X-ray $\theta/2\theta$ diffraction spectra of the FePt (30 nm)/Ag (175 nm)/Si thin films deposited at (a) 25°C, (b) 75°C and (c) 300°C.

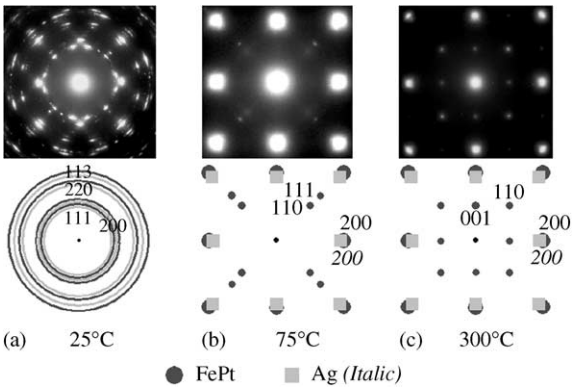

Fig. 11. The TEM diffraction pattern and simulated patterns of the FePt (30 nm)/Ag (175 nm)/Si thin films deposited at (a) 25°C, (b) 75°C and (c) 300°C. (Fig. 11(b) and (c) are enlarged to show the ordered reflections. Fig. 11(b) and (c) employ a different camera length from Fig. 11(a).)

25°C indicates that the epitaxial growth of the FePt and Ag layers is not very good, which is consistent with the results suggested by the X-ray $\theta/2\theta$ diffraction spectra in Fig. 10. In addition, no $L1_0$ ordered reflections are observed. This indicates that FePt film is FCC disordered as deposited at 25°C.

As the substrate temperature is increased to 75°C, the Ag underlayer is observed to grow

epitaxially on the Si (0 0 1) substrate and become (0 0 2) oriented (Fig. 11(b)). Furthermore, the Ag (0 0 2) oriented underlayer induces epitaxial growth of the $L1_0$ ordered FePt (0 0 2) thin film, indicated by the four FePt 110 reflections observed in the TEM diffraction pattern of Fig. 11(b). The low intensity of the 110 reflections implies that the $L1_0$ ordering at 75°C is very weak. The overlap of the FePt and Ag (0 0 2) reflections in the diffraction pattern indicates a small lattice misfit between the FePt (0 0 1) and Ag (0 0 1) planes. In addition, FePt 111 fundamental reflections are also observed in Fig. 11(b). These apparently arise from a few (1 1 2) oriented grains at this temperature.

At 300°C, no FePt 111 reflections are observed in the TEM diffraction pattern (see Fig. 11(c)). The epitaxial growth of FePt, as induced by the Ag underlayer, is clearly improved with increasing substrate temperature. While the TEM diffraction pattern at 75°C showed only $L1_0$ (0 0 1) variant formation, both of the $L1_0$ FePt 110 and 001 reflections are observed in the TEM diffraction pattern at 300°C (Fig. 11(c)). This indicates that the $L1_0$ FePt thin film deposited at 300°C has its *c*-axis distributed equally along the [1 0 0], [0 1 0] and [0 0 1] directions of the single crystal Si substrate. The presence of the $L1_0$ (0 0 1), (0 1 0) and (1 0 0) variants at 300°C implies that the (0 1 0) and (1 0 0) variants with easy axes parallel to the film plane are formed at higher substrate temperatures than 75°C. It can also be seen that the intensity of the $L1_0$ FePt reflections is stronger at 300°C than at 75°C. This demonstrates that the FePt thin film is more $L1_0$ ordered when prepared at 300°C than at 75°C.

In addition, the intensity of the 110 reflections from the 30 nm FePt film deposited at 75°C is weaker than that of the 5 nm FePt film deposited at 300°C. This result indicates that the thick FePt film deposited at 75°C is less $L1_0$ ordered than the thin FePt film prepared at 300°C (Fig. 8(a)).

The $\theta/2\theta$ X-ray diffraction spectra of the (a) FePt (30 nm)/Pt (12.5 nm)/Ag (175 nm)/Si and (b) FePt (30 nm)/Ag (175 nm)/Si thin films deposited at 300°C are shown in Fig. 12. The $L1_0$ FePt (0 0 1) X-ray diffraction peak intensity is significantly decreased when the Pt intermediate layer is deposited between the FePt and Ag layers. The

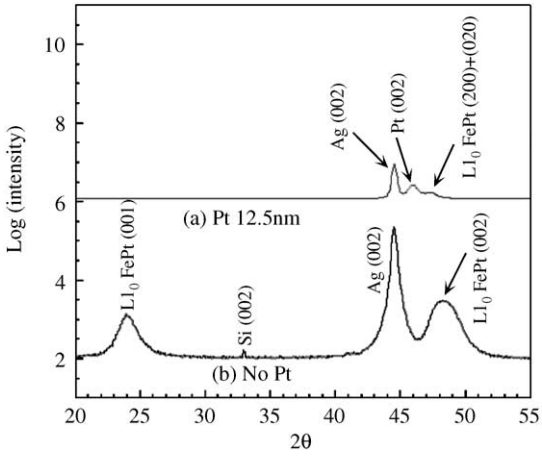

Fig. 12. The X-ray $\theta/2\theta$ diffraction spectra of the (a) FePt (30 nm)/Pt (12.5 nm)/Ag (175 nm) and (b) FePt (30 nm)/Ag (175 nm) thin films deposited onto the Si (0 0 1) substrates at 300°C.

decreased intensity of the $L1_0$ FePt (0 0 1) peak indicates that the amount of the $L1_0$ FePt (0 0 1) variant was reduced as the Pt intermediate layer is added. There are two possible explanations for the weak $L1_0$ FePt (0 0 1) peak. One possibility is that the FePt thin film is FCC disordered in its as-deposited state. The other possibility is that the FePt thin film becomes (1 0 0) or (0 1 0) textured as indicated by Fig. 3.

The TEM diffraction pattern of the FePt (30 nm)/Pt (12.5 nm)/Ag (175 nm)/Si thin film is shown in Fig. 13. The superlattice reflections resulting from the $L1_0$ ordered phase are observed in the TEM diffraction pattern. This indicates that the FePt thin film deposited onto the Pt intermediate layer is $L1_0$ ordered. If the FePt thin film is composed of an equal amount of the (1 0 0), (0 1 0) and (0 0 1) variants, the 001 and 110 reflections intensity ratio should be about 1:1.11.[1] In Fig. 13, the intensity of the 001 reflection is seen to be much larger than that of the 110 reflection. This indicates that the FePt thin film using the Pt intermediate layer has more (1 0 0) and (0 1 0) variants than (0 0 1) variants, which is also consistent with the results of the X-ray $\theta/2\theta$ diffraction scan in Fig. 12. From the results of

[1] Courtesy of Mr. Sangki Jeong, Carnegie Mellon University, Pittsburgh.

the X-ray and TEM diffraction we see that although the FePt films are still atomically ordered, the use of Pt intermediate layers changes the FePt texture from (0 0 1) to (1 0 0) and (0 1 0).

3.3. Mechanism of FePt $L1_0$ ordering and texture development

The FePt $L1_0$ ordering is accompanied by changes of the lattice parameters of the FePt unit cell. In order to investigate the FePt $L1_0$ ordering with the use of the Ag underlayer and the Pt intermediate layer, it is essential to measure the FePt lattice parameters. The variations of the FePt lattice parameters with the FePt and Ag thickness, substrate temperature as well as the use of the Pt intermediate layer are discussed in the following three sections.

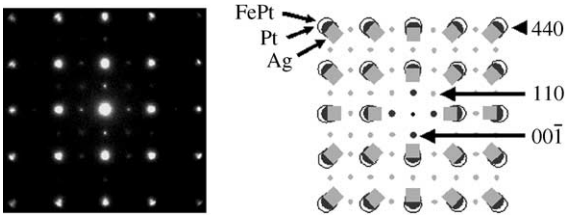

Fig. 13. The TEM selected area diffraction pattern and simulated pattern of the FePt (30 nm)/Pt (12.5 nm)/Ag (175 nm)/Si film deposited at 300°C.

3.3.1. Eects of FePt and Ag thickness

Fig. 14 shows the FePt (2 0 0), (0 2 0) and (0 0 2) inter-planar spacings of the (a) FePt (30 nm)/Ag (175 nm), (b) FePt (2.5 nm)/Ag (175 nm), (c) FePt (30 nm)/Ag (10 nm) and (d) FePt (30 nm) thin films deposited at 300°C onto the HF-etched Si substrates. For the cases of samples a, b and c, the interplanar spacings were obtained from the FePt (0 0 2) peaks of the in-plane X-ray diffraction methods described in the experimental procedures. For sample d, the FePt (0 0 2) peak is not observed because the FePt thin film deposited directly onto a Si substrate is (1 1 1) textured. The FePt inter-planar spacing of sample d was calculated from the lattice parameter obtained from the FePt (1 1 1) peak position shown in Fig. 7(a).

The 2.5 nm FePt film deposited onto the Ag underlayer (sample (b)) has larger (2 0 0) and (0 2 0) inter-planar spacings as well as a smaller (0 0 2) inter-planar spacing compared to the FePt thin film directly deposited onto the Si substrate (sample (d)). Ag has a 7.1% larger unit cell than FePt as shown in Fig. 2. It is hypothesized that the in-plane axes of the FePt unit cell is expanded by the Ag underlayer when the Ag underlayer induces the FePt epitaxial growth. The expansion of the FePt *a*- and *b*-axis leads the contraction of the FePt *c*-axis. Since $L1_0$ FePt has a smaller *c*-axis than the *a*- and *b*-axis, this favors the formation of the FePt $L1_0$ (0 0 1) variant. This explains why the

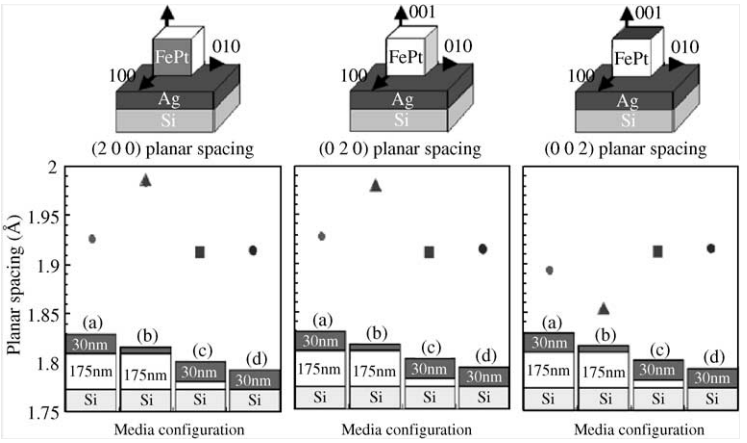

Fig. 14. The FePt (2 0 0), (0 2 0) and (0 0 2) inter-planar spacings of the (a) FePt (30 nm)/Ag (175 nm), (b) FePt (2.5 nm)/Ag (175 nm), (c) FePt (30 nm)/Ag (10 nm) and (d) FePt (30 nm) thin films deposited at 300°C onto the HF-etched Si substrates.

strong $L1_0$ FePt 110 reflections are observed in the TEM diffraction pattern shown in Fig. 8(a).

For the 30 nm thick FePt film using a Ag underlayer (sample (a) in Fig. 14), it can be observed in Fig. 8(b) to have not only the $L1_0$ (0 0 1) variant but also the $L1_0$ (1 0 0) and (0 1 0) variants. This indicates that the $L1_0$ (1 0 0) and (0 1 0) variants form *after* the (0 0 1) variant. Hence, it is hypothesized that the $L1_0$ (0 0 1) variant forms first due to the in-plane expansion of the FePt lattice by the Ag underlayer. The $L1_0$ (1 0 0) and (0 1 0) variants form later to lower the overall strain energy which results from the $L1_0$ (0 0 1) variant [10].

In addition, the FePt (2 0 0), (0 2 0) and (0 0 2) inter-planar spacings of the FePt thin film deposited onto the 10 nm Ag underlayer (sample (c)) are about the same as those of the FCC FePt thin film directly deposited onto the Si substrate (sample (d)). In other words, the FePt film deposited onto the thin Ag underlayer is not contracted along the film normal direction. The TEM plane-view bright field image of the FePt (30 nm)/Ag (10 nm) thin film shows a particle-like microstructure in Fig. 15. It is therefore hypothesized that this particle-like microstructure releases the strain energy due to the lattice misfit between the FePt and Ag layers. Hence, the FePt thin film is not contracted and does not form the (0 0 1) oriented $L1_0$ grains with the use of thin Ag underlayer as shown in Fig. 9. On the other hand, the FePt thin film deposited onto the thick 175 nm Ag underlayer is shown to be a continuous film (Fig. 15). The continuous FePt thin film is contracted along the film normal direction (Fig. 14) and induces strong $L1_0$ ordering (Fig. 8(b)).

The TEM diffraction pattern in Fig. 7 shows that the FePt thin film directly deposited onto the Si substrate at 300°C is FCC disordered. This may be because the [0 0 1] axis of the FePt thin film is not contracted in the absence of the Ag underlayer and therefore it does not form the $L1_0$ ordered phase.

3.3.2. *Eects of substrate temperatures*

The (0 0 2), (0 2 0) and (2 0 0) inter-planar spacings of the 30 nm FePt thin films deposited onto the 175 nm Ag underlayers at various substrate temperatures are plotted in Fig. 16. As seen in Fig. 16, the FePt (2 0 0) and (0 2 0) inter-planar spacings increase and (0 0 2) inter-planar spacing decreases with increasing substrate temperature. This indicates that the FePt [1 0 0] and [0 1 0] lattice parameters are expanded and [0 0 1] lattice parameter is contracted at high substrate temperature. As shown in Fig. 11(b), the FePt thin film has good epitaxial growth induced by the Ag underlayer at 75°C. During epitaxial growth, the Ag underlayer which has a unit cell 7.1% larger than FePt may expand the FePt [0 1 0] and [1 0 0] axes. This in-plane expansion causes the shrinkage of the FePt [0 0 1] axis which is perpendicular to the film plane. It is hypothesized that this distortion of the FePt unit cell may result in enhancing the FePt $L1_0$ ordering and aiding the formation of the $L1_0$ (0 0 1) FePt variant with easy axis perpendicular to the film plane at 75°C.

As the substrate temperature increases from 75°C to 300°C, the FePt (0 0 2) inter-planar spacing decreases and the FePt (2 0 0) and (0 2 0) inter-planar spacings increase. This indicates that the FePt [0 0 1] axis is further contracted and the [1 0 0] and [0 1 0] axes are further expanded with increasing substrate temperatures. This appears to cause even more $L1_0$ FePt ordering and more $L1_0$ FePt (0 0 1) variant as shown in the X-ray $\theta/2\theta$ diffraction spectra in Fig. 10. As more $L1_0$ FePt

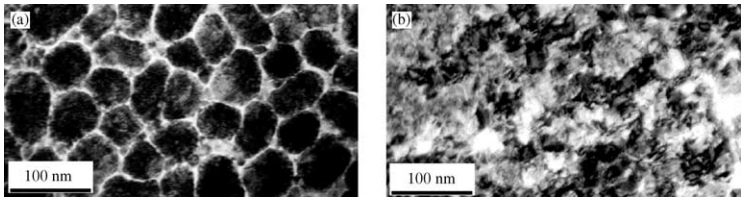

Fig. 15. TEM bright-field images of the (a) FePt (30 nm)/Ag (10 nm) and (b) FePt (30 nm)/Ag (175 nm) thin films.

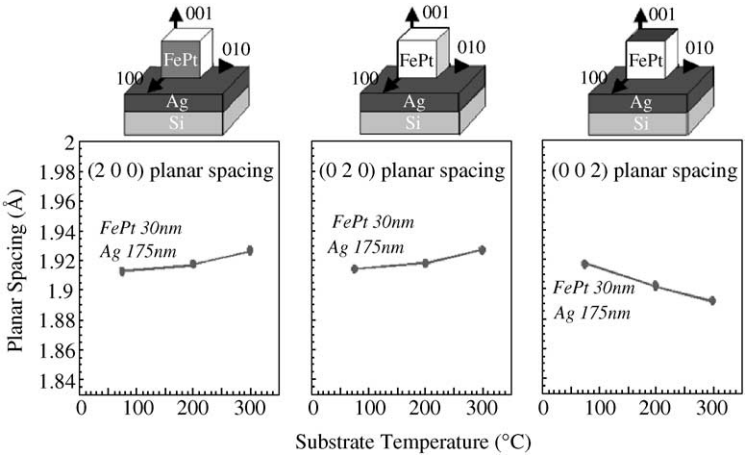

Fig. 16. The (2 0 0), (0 2 0) and (0 0 2) inter-planar spacings of FePt thin films deposited onto 175 nm Ag underlayers at various substrate temperatures.

Table 1
The (1 0 0), (0 1 0) and (0 0 1) inter-planar spacings of the FePt thin films deposited onto 175 nm Ag underlayer at 300°C with no intermediate layer as well as with the Pt intermediate layer

Plane of FePt	Planar spacing of FePt/Ag film (Å)	Planar spacing of FePt/Pt/Ag film (Å)
(1 0 0)	3.75	3.74
(0 1 0)	3.76	3.76
(0 0 1)	3.71	3.72

(0 0 1) variant is present, the $L1_0$ (1 0 0) and (0 1 0) variants may begin to grow in order to relax the strain energy resulting from the $L1_0$ FePt (0 0 1) variant [10]. As a consequence, the FePt thin film deposited at 300°C has its *c*-axis distributed equally along the [1 0 0], [0 1 0] and [0 0 1] directions of the single crystal Si substrate as shown earlier in the TEM diffraction pattern (See Fig. 8(b)).

3.3.3. Eects of Pt intermediate layer

Because the $L1_0$ FePt (0 0 1) peak intensity is strong enough to be observed in the in-plane X-ray diffraction spectra for both the FePt (30 nm)/Ag (175 nm) and FePt (30 nm)/Pt (12.5 nm)/Ag (175 nm) thin films, the (0 0 1) inter-planar spacing is investigated instead of the (0 0 2) inter-planar spacing. The changes of the (0 0 1), (0 1 0) and (0 0 1) inter-planar spacings of the FePt thin films using the Pt intermediate layer are shown in Table 1.

Compared to the FePt film without an intermediate layer, the FePt thin films deposited onto the Pt intermediate layer have a larger (0 0 1) inter-planar spacing. This indicates that the FePt thin film deposited onto the Pt intermediate layer is not contracted along the film normal direction as much as that deposited directly onto the Ag underlayer. This is due to the smaller lattice misfit of the FePt with Pt (2.6%) unit cell than that with the Ag (7.1%) unit cell. Hence, the FePt thin film using the Pt intermediate layer has a smaller amount of the $L1_0$ (0 0 1) variant than that without the Pt intermediate layer.

3.4. FePt thin film magnetic properties

The in-plane and perpendicular hysteresis loops of the FePt films are shown in Fig. 17. The FePt (30 nm)/Ag (175 nm)/Si thin film deposited at room temperature (Fig. 17(a)) as well as the FePt (30 nm)/Ag (10 nm)/Si (Fig. 17(b)) and FePt (30 nm)/Si thin film deposited at 300°C (Fig. 17(c)) show low in-plane coercivity due to the FCC disordered phase present in the film. The reversible rotation of the magnetization vector is observed when the magnetic field is applied perpendicular to the film plane. This is indicated by the rounded

magnetization curve shoulders of the perpendicular loop. The open region of the perpendicular loop most likely reflects wall motion of the magnetization. The FePt (30 nm)/Ag (175 nm) thin film deposited at 300°C (Fig. 17(d)) has a high coercivity due to high anisotropy energy associated with the $L1_0$ ordered phase. The *c*-axis is nearly equally distributed along the three [0 0 1], [0 1 0] and [1 0 0] axes. Thus the difference in the in-plane and perpendicular loops is less pronounced. For thin FePt (2.5 nm) shown in Fig. 17(e), the in-plane loop is almost closed. The perpendicular coercivity is higher than the in-plane coercivity because only the (0 0 1) variant is present in the thin film.

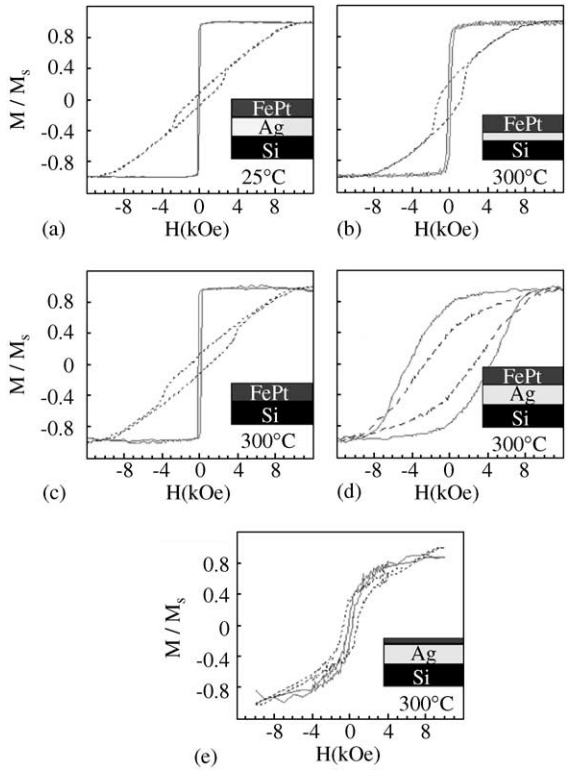

Fig. 17. The hysteresis loops of the (a) FePt (30 nm)/Si film deposited at 300°C, (b) FePt (2.5 nm)/Ag (175 nm)/Si film deposited at 300°C, (c) FePt (30 nm)/Ag (175 nm)/Si film deposited at 25°C, (d) FePt (30 nm)/Ag (10 nm)/Si film deposited at 300°C, and (e) FePt (30 nm)/Ag (175 nm)/Si film deposited at 300°C. (Solid line: in-plane loop and dotted line: perpendicular loop.)

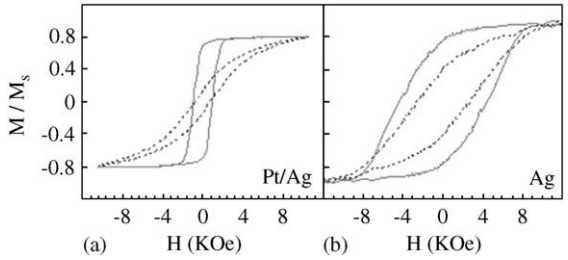

Fig. 18. The hysteresis loops of the (a) FePt (30 nm)/Pt (12.5 nm)/Ag (175 nm) and (b) FePt (30 nm)/Ag (175 nm) thin films deposited onto the single crystal Si at 300°C. (Solid line: in-plane loop and dotted line: perpendicular loop.)

The effects of using the Pt intermediate layer on the FePt magnetic properties are shown in Fig. 18. The FePt magnetic layer using the Pt intermediate layer (Fig. 18(a)) has smaller in-plane and perpendicular coercivities than that without the Pt intermediate layer (Fig. 18(b)). Compared to the FePt thin film directly deposited onto the Pt intermediate layer, the contraction along the sample normal direction of the FePt films deposited onto the Ag underlayer was found more severe (see Table 1). This may result in more $L1_0$ FePt phase formation in the FePt/Ag thin film than in the FePt/Pt/Ag thin films. Hence, the in-plane and perpendicular coercivities of the FePt/Pt/Ag thin film were smaller than those of the FePt/Ag thin film as shown in Fig. 18.

4. Conclusion

FePt thin films directly deposited onto HF-etched single crystal Si substrates are (1 1 1) textured and FCC disordered. On the other hand, the use of Ag underlayers has been shown to induce epitaxial growth of the FePt thin film. Because Ag has a slightly larger unit cell than FePt, the in-plane direction of the FePt unit cells were stretched by the Ag underlayers during epitaxial growth. This causes a contraction of the FePt unit cells along the plane normal direction, which enhances the $L1_0$ FePt ordering at reduced temperatures and forms the $L1_0$ (0 0 1) variant. In addition, it has been shown that the greater the

contraction of the FePt unit cell along the plane normal, the greater the tendency for the $L1_0$ FePt phase to form.

FePt has smaller lattice misfit with the Pt unit cell. The FePt thin films deposited onto the Pt intermediate layer were shown to be contracted less along the sample normal direction than that directly deposited onto the Ag underlayer. As a result, the FePt/Pt/Ag thin films have less $L1_0$ (0 0 1) variant than (1 0 0) and (0 1 0) variants.

Acknowledgements

The authors gratefully thank Dr. B. Lu and Dr. T. Klemmer in Seagate Research for valuable discussions. This research is supported by CMU Data Storage Systems Center under an NSF grant No. ECD-89-07068.

References

[1] P.-L. Lu, S.H. Charap, IEEE Trans. Magn. 30 (6) (1994) 4230.
[2] T. Klemmer, D. Hoydick, H. Okumura, B. Zhang, W.A. Soffa, Scr. Metall. Mater. 33 (1995) 1793.
[3] K. Coffey, M.A. Parker, J.K. Howard, IEEE Trans. Magn. 31 (6) (1995) 2737.
[4] T.B. Massalski, Binary Alloy Phase Diagrams, ASM International, 1996.
[5] R.A. Ristau, K. Barmak, L.H. Lewis, K.R. Coffey, J.K. Howard, J. Appl. Phys. 86 (1999) 4527.
[6] P. Villars, L.D. Calvert, Pearson's Handbook of Crystallographic Data for Intermetallic Phases, ASM International, 1991.
[7] Wei Yang, D.N. Lambeth, Li Tang and D.E. Laughlin, J. Appl. Phys. 81 (1997) 4370.
[8] Y.N. Hsu, S. Jeong, D.N. Lambeth, D.E. Laughlin, J. Appl. Phys. 89 (2001) 7068.
[9] C. Hammond, The Basics of Crystallography and Diffraction, International Union of Crystallography, Oxford Science Publication, Oxford, 1997.
[10] Bing Zhang, Thesis Dissertation, University of Pittsburgh, 1991.